Dual thermoresponsive polysaccharide derivative – water system. Partially substituted amylose butylcarbamate in water

Yuma Nakata,[a] Shinichi Kitamura,[b] and Ken Terao[*,a]

[a]*Department of Macromolecular Science, Graduate School of Science, Osaka University, 1-1 Machikaneyama-cho, Toyonaka, Osaka 560-0043, Japan*

[b]*Center for Research and Development of Bioresources, Organization for Research Promotion, Osaka Prefecture University, 1-2, Gakuen-cho, Naka-ku, Sakai 599-8570, Japan*

* Corresponding author.

Phone.: +81 6 6850 5461.

E-mail address: terao.ken.sci@osaka-u.ac.jp

ABSTRACT

Partially substituted amylose *n*-butylcarbamate (ABC) samples were synthesized with weight-average molar mass M_w ranging between 40 kg mol^{-1} and 220 kg mol^{-1} with different degree of substitution DS. When DS was between 0.17 and 0.33, the ABC samples were soluble in water. Furthermore, both LCST and UCST type phase separations were observed for the ABC samples in water when DS is greater than 0.26. The closed-loop phase diagrams for the dual thermoresponsive ABC samples in water were constructed by turbidity measurement. The UCST ranged from 70 °C to 77 °C and the LCST ranged from 13 °C to 17 °C. SAXS measurements were performed for dilute aqueous ABC solutions to determine the chain conformation of ABC at various temperatures. The resulting form factor at the polymer mass concentration of 3 mg mL^{-1} indicated that the chain conformation is almost independent of temperature, except for the chain diameter, which is influenced by the temperature-dependent hydration behavior. This result suggests that the attractive interactions between ABC chains are not very significant even between UCST and LCST, where higher concentrated polymer solutions show macroscopic phase separation.

Keywords: water soluble polysaccharide derivative; dual thermo-responsibility; UCST; LCST; small-angle X-ray scattering; inclusion complex

Abbreviations: A_2, second virial coefficient; ABC, amylose *n*-butylcarbamate; AEC, amylose ethylcarbamate; $A(R_{H,app})$, spectrum of $R_{H,app}$; c, polymer mass concentrations; d, diameter of the touched bead; $Đ$, dispersity index defined as the ratio of M_w to the number average molar mass; DMAC, *N,N*-dimethylacetamide; DLS, dynamic light scattering; DS, degree of substitution; ESA, enzymatically synthesized amylose; $g^{(2)}(t)$, autocorrelation function; h, helix rise per residue; K, optical constant of X-ray; L, contour length; LCST, lower critical solution temperature; L_K, Kuhn segment length; M_0, average molar mass of the repeat unit; M_w, weight-average molar mass; P, degree of polymerization; $P(q)$, form factor; PEO, polyethylene oxide; q, magnitude of the scattering vector; R, gas constant; R_g, radius of gyration; $R_{H,app}$, apparent hydrodynamic radius; R_q, reduced scattering intensity; SAXS, small-angle X-ray scattering; T, absolute temperature; T_{cloud}, cloud point temperature; UCST, upper critical solution temperature; $\bar{v}$, partial specific volume of the solute; z, number of moles of electrons per unit mass of the solute; $\Delta\overline{G_m}$, molar Gibbs energy of mixing; $\Delta I(q)$, excess scattering intensity; Δz, X-ray contrast factor; λ_0, wavelength in a vacuum; $\rho_{e,s}$, electron density of the solvent; ϕ, volume fraction of the polymer; χ, interaction parameter.

1. Introduction

The phase separation behavior of aqueous polymer solutions has been widely investigated as thermoresponsive polymers due to the fundamental interest in the thermodynamics of polymer-solvent systems as well as their versatile applications in the biomedical field (Liu, Fraylich, & Saunders, 2009; Roy, Brooks, & Sumerlin, 2013). Since hydration is a key factor in the dissolution of polymers in water, the lower critical solution temperature (LCST) is frequently observed in the phase diagram of polymer-water systems, whereas the upper critical solution temperature (UCST) is more common for polymer-organic solvent systems. Polyethylene oxide (PEO) has both LCST and UCST in water, and the UCST is higher than the LCST. It is called a closed-loop phase diagram, while the UCST of PEO was observed at high pressure and temperature, which is much higher than the boiling temperature of water at atmospheric pressure (Saeki, Kuwahara, Nakata, & Kaneko, 1976). The closed-loop phase diagram for aqueous polymer solution systems at atmospheric pressure has been reported for some synthetic homopolymers (Audureau, Coumes, Rieger, & Stoffelbach, 2022; Cai, Zhong, Su, Lin, & He, 2015; Li, He, Ling, & Tang, 2017; Longenecker, Mu, Hanna, Burke, & Stover, 2011; Okamura et al., 2002) and random copolymers (Shiomi, Imai, Watanabe, & Miya, 1984; Zhu, Batchelor, Lowe, & Roth, 2016). Because of their potential use in biomedical applications, it is worthwhile to develop such polymers with dual thermo-responsiveness from naturally derived macromolecules including polysaccharides.

Polysaccharide derivatives can be a candidate for functional water-soluble polymers because the polar groups, including OH, are readily chemically modified in the mild conditions. While LCST-type phase transition behaviors of aqueous solutions have been found for many polysaccharide derivatives, i.e., cellulose ethers (Bizmark et al., 2022; Chevillard & Axelos, 1997; Heymann, 1935; McAllister, Schmidt, Dorfman, Lodge, & Bates, 2015; Nishida et al., 2017; Sarkar, 1979), starch derivatives (B. Ju, Cao, & Zhang, 2013; B. Z. Ju, Yan, & Zhang,

2012), chitosan derivatives (Chen, Zhang, Zhang, Wang, & Ren, 2022), and dextran derivatives (Otto, Marina, Zhou, & Blencowe, 2021), dual temperature responsible polysaccharide derivatives with closed-loop phase diagram have not been found, to our knowledge, except for specially designed polysaccharide complexes (Phunpee, Ruktanonchai, & Chirachanchai, 2022) in which the thermoresponsive nature is maintained by the synthetic polymer chains grafted to the polysaccharide backbones. Furthermore, although a sol-gel-sol transition of aqueous xyloglucan solution was observed with increasing temperature (Shirakawa, Yamatoya, & Nishinari, 1998), it should be distinguished from phase separation. Recently, we reported that LCST-type phase separation behavior was observed for partially substituted amylose ethylcarbamate (AEC) derivatives with degree of substitution (DS) between 0.9 and 1.3 (Kimura, Kochi, Kitamura, & Terao, 2020). As a first step of this study, we found that low DS (~0.3) amylose butylcarbamate exhibits LCST-type phase separation behavior and becomes soluble in water with increasing temperature, suggesting a closed-loop phase diagram or dual thermo-responsibility. It can be the first example of achieving dual thermoresponsive phase separation behavior for a polysaccharide derivative in aqueous solution. Although there are few polysaccharide derivatives with closed-loop phase diagrams in aqueous media, and therefore few applications at present, it can be an important material to consider biodegradability and biocompatibility. We therefore synthesized partially substituted amylose *n*-butylcarbamate (ABC) samples with different DS and chain length to investigate the phase diagram of the aqueous solutions. Small-angle X-ray scattering (SAXS) was also conducted to clarify the chain conformation in dilute aqueous solution over a wide temperature range, including the temperature between LCST and UCST. Because the resulting ABC samples have relatively low DS of about 0.3, the iodine test was also examined to elucidate the ability of the ABC samples to form inclusion complexes. The data were compared with those of previously investigated AEC samples. Taking into account that the current reaction to evaluate carbamate

derivatives can be applied to versatile polysaccharides and furthermore the current thermoresponsiveness was maintained at relatively low degree of substitution (~0.3), meaning that butyl carbamate group is necessary only one for the three anhydrous glucose unit, the current result can be an important suggestion to find out the unknown thermoresponsive polysaccharide derivatives for which the physical nature, that is, the inclusion complex formation ability, is similar to the original polysaccharides.

2. Experimental section

2.1. ABC samples

Two enzymatically synthesized amylose (ESA) samples **ESA50K** and **ESA200K** prepared in the manner reported previously (Kitamura, Yunokawa, Mitsuie, & Kuge, 1982) were chosen in this study. Six ABC samples with different DS and chain length were prepared in the similar manner for the AEC samples reported previously (Kimura et al., 2020) from enzymatically synthesized amylose as illustrated in Fig. S1 in the Supporting Information. A procedure to prepare an ABC sample, **ABC40K0.32**, is as follows.

A 2.5 g powder sample of **ESA50K** (15 mmol in the repeat unit) with a molar mass of 50 kg mol^{-1} was placed in a glass flask with 2.5 g LiCl. The mixture was heated to 90 °C in an oil bath under a vacuum for 3 h to remove a small amount of water. *N,N*-dimethylacetamide (DMAC, super dehydrated grade, 80 mL) was added to the flask under an Ar atmosphere to dissolve the ESA sample in the solvent (DMAC-LiCl). Pyridine (80 mL) distilled over CaH_2 and *n*-butyl isocyanate (1.2 mL, 14 mmol) was added to the mixture. The resulting reaction solution was mixed at 90 °C for 24 h. The brown colored solution was poured into acetone (2 L) to precipitate the polymer sample. The evaluated sample was dissolved in water and dialyzed against water for at least 4 d with a SPECTRA/POR dialysis tube (MWCO = 12000 -

14000). The resulting aqueous solution was lyophilized to obtain a white solid sample. The yield was 1.97 g. Since ABC samples with high DS (0.8 – 0.9) were not soluble in water, the crude sample was purified by reprecipitation with methanol as solvent and water as precipitant.

The chemical structure of the obtained ABC samples was confirmed by the ultimate analysis and ^{1}H NMR with dimethyl sulfoxide-d_6 as a solvent (Fig. S2). The DS value was estimated from the weight ratio of carbon to nitrogen from the former analysis. The purified ABC samples synthesized from **ESA50K** were designated as **ABC40K0.17**, **ABC40K0.32**, **ABC40K0.33**, and **ABC40K0.83**. The other two ABC samples prepared from **ESA200K** were named as **ABC220K0.27** and **ABC220K0.92**, where 40K and 220K indicate an approximate value of the weight average molar mass M_w. The DS value is shown as the last digits of the sample code. **ABC40K0.17**, **ABC40K0.32**, **ABC40K0.33**, and **ABC220K0.27** were soluble in cold water, while aqueous solutions of **ABC40K0.32**, **ABC40K0.33**, and **ABC220K0.27** were thermosensitive. The high DS samples, **ABC40K0.83** and **ABC220K0.92**, were, however, not soluble in water. We did not determine the molar mass dispersity of the samples because the appropriate solvent for size-exclusion chromatography was not found. Considering that a similarly prepared fully substituted butylcarbamate sample from **ESA50K** (ATBC148K) has a molar mass dispersity $Đ$ = 1.14, defined as the ratio of M_w to the number average molar mass (Kabata, Ryoki, Kitamura, & Terao, 2021), it is suggested that the current ABC40K samples have a relatively narrow molar mass dispersity. The sample characteristics are summarized in Table 1. The yield was calculated from the weight ratio of the purified ABC sample to the added ESA sample taking into account the weight increase of the substitution reaction. The M_w values for three thermoresponsive polymers were determined from the SAXS measurements described below. Although the M_w values for the other samples were not determined, they were calculated from the M_w value for the other samples from the same ESA source, assuming the same degree of polymerization (DP).

Table 1

Molecular characteristics of ABC samples in water

	Yield /%	DS [a]	M_w / kg mol^{-1}	Solubility in water [e]
ABC40K0.17	71	0.17	37 [c]	S
ABC40K0.32	66	0.32	40.7 [b]	P
ABC40K0.33	54	0.33	39.3 [b]	P
ABC40K0.83	61	0.83	52 [c]	I
ABC220K0.27	56	0.27	290 [d]	P
ABC220K0.92	80	0.92	220 [b]	I

[a] DS = 3 for full substitution.

[b] From SAXS,

[c] Calculated assuming the same DP as **AEC40K0.32** and **ABC40K0.33**.

[d] Calculated assuming the same DP as **AEC220K0.92**.

[e] I: insoluble. S: soluble between 4 and 80 °C. P: phase separation was observed.

2.2. Light and X-ray scattering measurements

Synchrotron-radiation SAXS measurements were conducted for the three thermoresponsive ABC samples, **ABC40K0.32**, **ABC40K0.33**, and **ABC220K0.27**, in water at different temperatures between 10 °C and 80 °C at the BL40B2 beamline in SPring-8 (Hyogo, Japan). The wavelength λ_0 in a vacuum and the sample-to-detector distance were chosen as 0.10 nm and 4.2 m, respectively. A 2 mmϕ quartz capillary fixed in a specially designed aluminum block was utilized both for aqueous ABC solutions with 3 or 4 different polymer mass concentrations c and the solvent to properly subtract the scattering intensity of the solvent

from that of the solution. The capillary cell was installed into a thermostatic cell holder equipped with a Peltier element for temperature control. A Dectris Pilatus 3 2M photon counting detector was utilized to obtain the two-dimensional scattering data. The diffraction data of silver behenate were acquired to accurately estimate the beam center and sample-to-detector distance. A SAngler software (Shimizu et al., 2016) was utilized to calculate the scattering intensity as a function of the magnitude q of the scattering vector. The resulting scattering intensity was normalized by the intensity of the incident light. The excess scattering intensity $\Delta I(q)$ was evaluated as the difference of the normalized scattering intensity between the solution and the solvent at each q. The repeatability of the scattering data was confirmed that $\Delta I(q)/c$ was essentially independent of c for different concentrations. The ratio R_q/K of the reduced scattering intensity R_q to the optical constant K of X-ray was estimated from the following relationship, with the subscript r being the reference value evaluated from a TOSOH polyethylene oxide standard sample (M_w = 37.6 kg mol^{-1}, $Đ$ = 1.14) (Glatter & Kratky, 1982)

$$\frac{R_q}{K} = M_{\mathrm{w,r}} \left(\frac{c_\mathrm{r}}{\Delta I_\mathrm{r}(q)} \right)_{\substack{c_\mathrm{r}\to 0 \\ q\to 0}} \frac{\Delta z_\mathrm{r}^2}{\Delta z^2} \Delta I(q) \qquad (1)$$

where the X-ray contrast factor Δz^2 is defined with the number of moles of electrons per unit mass of the solute z, the partial specific volume of the solute $\bar{v}$, and the electron density of the solvent $\rho_{\mathrm{e,s}}$ as $\Delta z \equiv z - \bar{v}\rho_{\mathrm{e,s}}$. The $\bar{v}$ values for the ABC samples in water were determined from the solution density by using an Anton Paar DMA 5000 densitometer.

Dynamic light scattering (DLS) measurement was examined for **ABC40K0.32** and **ABC40K0.17** in water with an ALV/SLS/DLS-5000 light scattering photometer. An Nd:YAG laser with λ_0 = 532 nm was utilized as an incident light. A solvent and ABC solutions were optically cleaned using a cellulose acetate filter with the pore size of 0.80 μm and then poured

into a cylindrical cell with 14 mm i.d. The autocorrelation function $g^{(2)}(t)$ of the scattering intensity was determined at different q. The CONTIN analysis was examined for the $g^{(2)}(t)$ data to estimate the apparent hydrodynamic radius $R_{H,app}$ and the spectrum $A(R_{H,app})$.

2.3. Iodine test and turbidity measurements

10 μL of a 0.05 M aqueous I_2-KI solution was added to 1.5 mL of an aqueous ABC solution with c = 5 mg mL^{-1}. UV-Vis spectra were measured for the mixed solution with a Jasco V-550 spectrometer using a rectangular quartz cell with 2 mm path length in the λ_0 range from 200 nm to 900 nm at different temperatures from 10 °C to 90 °C. The repeatability of the data was confirmed by multiple measurements with independent solutions.

Solution turbidity measurements were examined for aqueous solutions of **ABC40K0.32**, **ABC40K0.33**, and **ABC220K0.27** to determine the cloud point temperatures T_{cloud} both of LCST and UCST type phase separation using a Jasco V-750 spectropolarimeter and a Peltier temperature controller. The repeatability of the data was verified by measuring many polymer solutions at different concentrations. A rectangular quartz cell with 2 mm path length was placed into the thermostatic cell holder. The solution temperature was monitored using a thin probe immersed in the solution. Both the heating and cooling rates were set to be 0.5 °C/min. The wavelength λ_0 was chosen to be 550 nm or 800 nm without or with iodine, respectively.

3. Results and discussion

3.1. Solubility and molecular characteristics in water

ABC samples within the DS range between 0.17 and 0.33 are soluble in cold water whereas those with higher DS are insoluble in water. The DS range to dissolve ABC in water is narrower than that of the previously investigated ethylcarbamate derivative of amylose

(AEC) which was soluble in the range of DS < 1.3. This is most likely due to the higher hydrophobicity of the butyl group of ABC than the ethyl group of AEC.

Although each aqueous ABC solution is transparent at low temperatures, results from DLS for **ABC40K0.32** show that significant light scattering from aggregates larger than 100 nm was observed as shown in Fig. S3. Similar results were evaluated for **ABC40K0.17**. Although the scattering intensity from the large aggregate is more significant than that from the dispersed polymer molecules considering that the scattering intensity from each particle is proportional to the sixth power of the particle size, assuming the same density, it is reasonable to suppose that the weight fraction of the former aggregates is much lower than the latter dispersed polymer. Since the peak for the large aggregates appreciably decreases with increasing scattering angle comparing with the peak for the dispersed polymer molecules, the scattering intensity for the SAXS measurement with the larger q range is mainly from the dispersed polymer. Indeed, the q dependence of the excess scattering intensity $\Delta I(q)/c$ from SAXS measurement for the ABC samples in water shown in Fig. S4, mostly flat region is found around $q = 0.1$ nm^{-1}. We thus constructed a square root Zimm plot (Berry plot) for the ABC samples to extrapolate the scattering intensity to zero c and q to estimate M_w, the second virial coefficient A_2, the radius of gyration R_g, and the form factor $P(q)$. We note that $P(q)$ was not estimated for **ABC220K0.27** because the $\Delta I(q)/c$ at high q range were scattered. The Berry plots for **ABC40K0.32** in water at 10 °C and 80 °C are shown in Fig. 1. While abnormally high scattering intensity is observed at the low q end, especially at 10 °C, an appropriate linear region allows us to extrapolate the scattering intensity to zero q. The evaluated M_w from the double extrapolated values of $(Kc/R_q)^{1/2}$ to $q = 0$ and $c = 0$ for **ABC40K0.32** and **ABC40K0.33** at different temperatures were fairly consistent within 10%. The average M_w values were thus summarized in Table 2 with the radius of gyration R_g estimated from the initial slope at infinite dilution (blue filled circles) in the figure. Negative A_2 values were evaluated from the slope of

the $(Kc/R_q)^{1/2}$ data at $q = 0$. The resulting values range from -1×10^{-4} to -4×10^{-4} (mol m^{3}kg^{-2}), suggesting poor-solvent conditions.

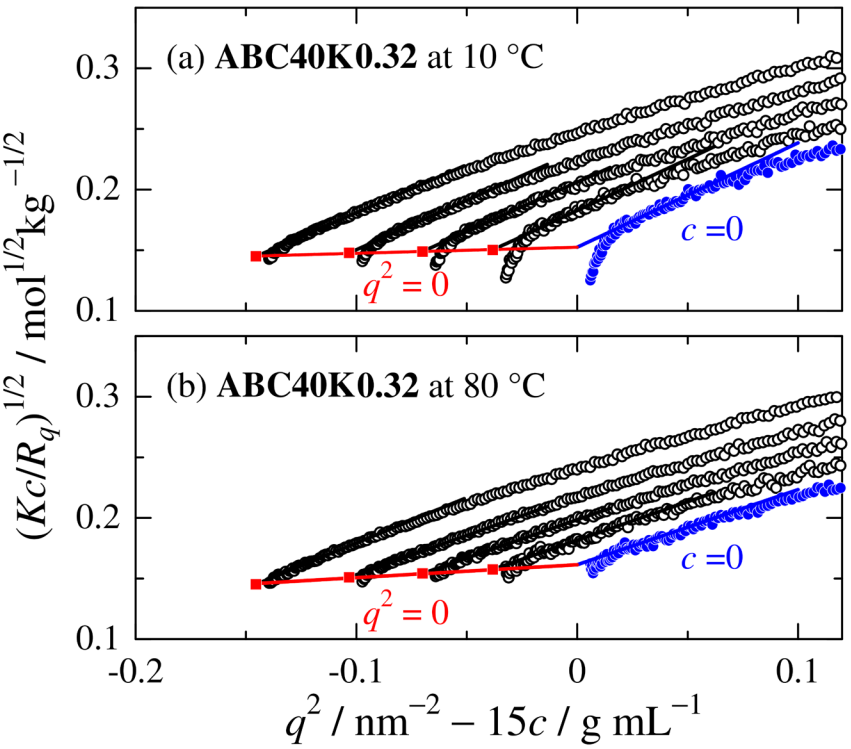

Fig. 1. Square-root Zimm plots (Berry plots) for **ABC40K0.32** in water at (a) 10 °C and (b) 80 °C. Filled circles and squares, extrapolated values to $c = 0$ and $q^2 = 0$, respectively.

Table 2

Radius of gyration R_g and critical point temperatures for ABC samples in water

	M_w / kg mol^{-1}	R_g / nm at 10 °C	R_g / nm at 80 °C	LCST / °C	UCST / °C
ABC40K0.32	40.7	5.8	4.8	17	76
ABC40K0.33	39.3	4.9	3.8	13	77
ABC220K0.27	220	9.0		15	70

Fig. 2 (a) shows the Holzer plots for **ABC40K0.32** and **ABC40K0.33** in water at 10 °C and 80 °C. The shape is similar to that of previously investigated AEC (Kimura et al., 2020) and amylose (Jiang, Kitamura, Sato, & Terao, 2017), indicating that the ABC chains behave as wormlike chains with medium or low chain stiffness. The $P(q)$ data were thus analyzed in terms of the touched bead wormlike chain model for which the theoretical $P(q)$ is expressed as (Burchard & Kajiwara, 1970; Yamakawa & Yoshizaki, 2016)

$$P(q) = 9\left(\frac{2}{qd}\right)^6\left(\sin\frac{qd}{2} - \frac{qd}{2}\cos\frac{qd}{2}\right)^2\left(\frac{2}{L^2}\right)\int_0^L (L-t)I(L_\mathrm{K}q; t/L_\mathrm{K})\mathrm{d}t \qquad (2)$$

where L, L_K, d, and $I(L_\mathrm{K}q; t/L_\mathrm{K})$ indicate the contour length, Kuhn segment length (a measure of the chain stiffness), diameter of the touched bead (a measure of the chain thickness), and the characteristic function. The numerical expression of Nakamura-Norisuye (Nakamura & Norisuye, 2004, 2008) was utilized to calculate the characteristic function $I(L_\mathrm{K}q; t/L_\mathrm{K})$ for the given wormlike chain parameters. The contour length L can be related to the helix rise per residue h with $L = hM_\mathrm{w}/M_0$, where M_0 is the average molar mass of the repeat unit. A curve fitting procedure was employed for the four $P(q)$ data to estimate the three parameters h, L_K, and d. For all the four cases, the h and L_K values are almost the same, that is, $h = 0.13 \pm 0.01$ nm and $L_\mathrm{K} = 4.2 \pm 0.1$ nm. The former parameter is somewhat smaller than that for fully substituted ABC in organic solvents (Terao et al., 2010), suggesting that hydrophobic interactions surrounding the amylosic main chain contribute to the contraction of the helical structure. A similar behavior was also found for single-chain schizophyllan derivative in aqueous media (Tomofuji, Yoshiba, Christensen, & Terao, 2019) and AEC (Kimura et al., 2020). Considering that the amylose chains in V-amylose, in which the amylose chain forms an inclusion complex with small molecules, can have a similar h value calculated from the unit cell parameter (Cardoso et al., 2007; Le et al., 2022; Nishiyama et al., 2010), the hydrophobic

butyl group can be located inside the helical structure. This suggestion is supported by the presence of a rigid helical structure in fully substituted amylose butylcarbamate in tetrahydrofuran. (Terao et al., 2012; Terao et al., 2010; Terao & Sato, 2018). On the other hand, the chain stiffness of ABC in water is similar to that of AEC (Kimura et al., 2020) and amylose (Jiang et al., 2017), showing high flexibility in water. The third parameter, d, however, appreciably depends on the temperature; that is, d = 1.9 nm at 10 °C and 1.0 – 1.3 nm at 80 °C. This difference may be related to the hydration of the ABC chains.

According to the Benoit-Doty expression (Benoit & Doty, 1953) for the wormlike chain, the R_g value for **ABC40K0.32** and **ABC40K0.33** is calculated to be 4.0 nm from h and L_K. Somewhat larger R_g value from the Berry plot in Table 2 is most likely due to the small amount of aggregation.

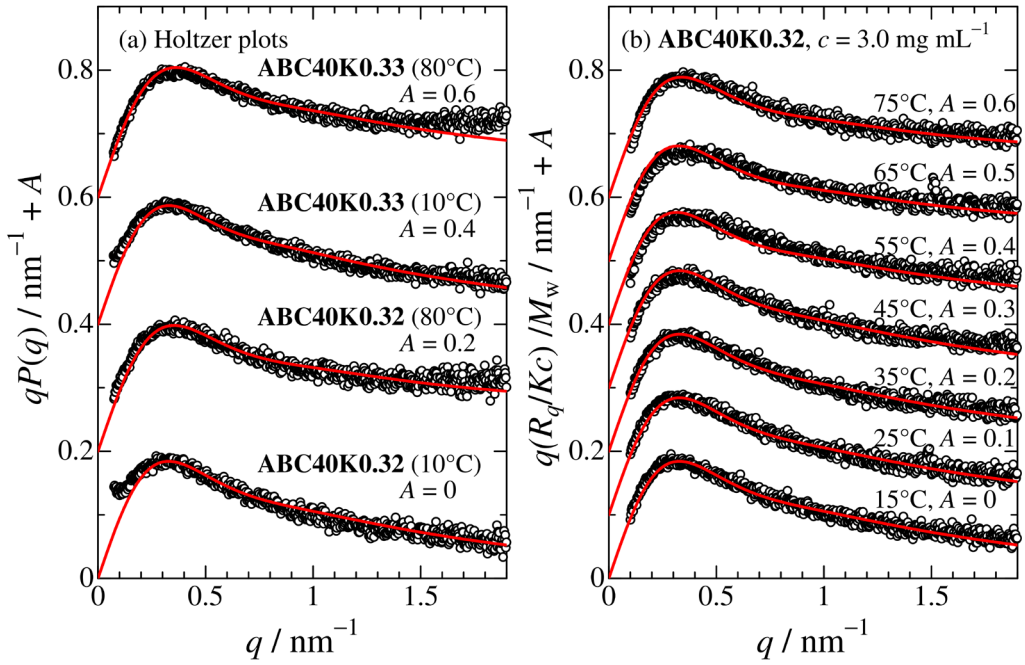

Fig. 2. (a) Holtzer plots [$qP(q)$ vs q] for the indicated ABC samples in water at 10 °C and 80 °C. (b) Holtzer plots for **ABC40K0.32** in water at different temperatures (c = 3 mg mL^{-1}). Solid curves, theoretical values for wormlike chains.

Although the scattering intensity can be influenced by the intermolecular interactions in general, almost no concentration dependence was seen for the current SAXS data in the q range above 0.15 nm^{-1} (Fig. S4). Thus, $q(R_q/Kc)/M_w$ for the ABC sample in water can be assumed to be the same as that for $qP(q)$ except for the low q range. Fig. 2(b) displays the plots for **ABC40K0.32** at c = 3.0 mg mL^{-1} at various temperatures. While the sample has both UCST and LCST phase separation behavior, all plots have substantially the same shape, indicating that this concentration is lower than the closed-loop phase boundary. In other words, no coil-globule transition is observed for the ABC sample in water at least for **ABC40K0.32** even between LCST and UCST. This is in contrast to the typical thermoresponsive polymers including poly(*N*-isopropylacrylamide) (Wang, Qiu, & Wu, 1998; Wu & Wang, 1998), for which phase boundary concentration of the dilute phase is extremely low above LCST (Han, Takahashi, Kuang, & Sato, 2022), suggesting that attractive interactions between the polymer segments of ABC samples in water are not very significant even between LCST and UCST.

The wormlike chain parameters h, L_K, and d were estimated at each temperature. While the resulting h and L_K values were mostly independent of the temperature, the chain thickness gradually decreased from 1.9 nm to 1.0 nm between 45 °C and 75 °C with increasing temperature. The Kuhn segment number L/L_K is calculated from the parameters to be 6.8. According to the previous analyses of various flexible and semiflexible polymers (Norisuye & Fujita, 1982; Norisuye, Tsuboi, & Teramoto, 1996), the excluded volume effect is insignificant at the L/L_K value. Therefore, the essentially temperature independent dimensional properties of the ABC sample in water are reasonable.

3.2. Phase separation behavior of aqueous solution

Aqueous solutions of the three thermoresponsive ABC samples, **ABC40K0.32**, **ABC40K0.33**, and **ABC220K0.27** show both LCST and UCST type phase separation behavior.

To construct the phase diagram, that is, temperature-concentration relationship of the phase boundary, optical transmittance measurements were examined both for heating and cooling processes. Fig. 3(a) and (b) show the typical results of the measurements. The transmittance significantly reduces at the phase separation temperature. The cloud point temperature T_{cloud} was defined as the temperature at which the transmittance reduced to 90 % of the initial solution. With further temperature changes, the transmittance reascends. This is likely due to both macroscopic phase separation and a re-elevation of solubility, taking into consideration that the absolute value of the transmittance is not a direct measure of insolubility. The resulting cloud point curves are shown in Figs. 3 (c) and (d). Due to the limitations of our experimental equipment, transmittance measurements above 85 °C were challenging. As a result, the T_{cloud} for UCST phase separation could not be determined for some solutions, particularly those at low concentrations. Even in this case, significant reduction of the transmittance was observed with decreasing temperature, indicating that the phase boundary concentration is close to 80 °C. We thus roughly estimated both critical point temperatures LCST and UCST from the lowest and highest T_{cloud}, respectively as shown in Table 2. Fig. 3(c) compares the phase diagram for **ABC40K0.32** and **ABC40K0.33**. The M_{w} values of the two samples are substantially the same and the DS values are slightly different. Even though the DS difference cannot be confirmed from the current method, appreciable difference can be recognized especially for the lower phase boundaries. Considering that the solubility of ABC samples reduces with increasing DS as shown in Table 1, wider biphasic region for the higher DS sample (**ABC40K0.33**) suggests that an increase of the butyl carbamate group increases hydrophobicity of ABC.

According to the Flory-Huggins theory, the molar Gibbs energy of mixing $\Delta\overline{G_{\mathrm{m}}}$ can be expressed as

$$\Delta\overline{G_{\mathrm{m}}} = RT\left[(1-\phi)\ln(1-\phi) + \frac{\phi}{P}\ln\phi + \chi\phi(1-\phi)\right] \qquad (3)$$

where R, T, ϕ, P, and χ denote the gas constant, absolute temperature, volume fraction of the polymer, degree of polymerization, and interaction parameter, respectively. The reduction of hydrophobicity corresponds to decreasing χ. Although this equation predicts wider biphasic region for the higher P, we do not have different molar mass samples with the same DS. Fig. 3(d) thus makes the comparison of the phase diagram for **ABC40K0.32** and **ABC220K0.27**. Even though the latter sample has lower DS, namely, lower χ value, resulting in a decrease in $\Delta\overline{G_{\mathrm{m}}}$, the higher molar mass of **ABC220K0.27** increases $\Delta\overline{G_{\mathrm{m}}}$. As a result, the phase boundary concentrations of these two samples are substantially the same. Another important point to note is that the temperature-insensitive molecular conformation, as described above, suggests that the increase of χ with rising temperature due to dehydration is not very significant for the current ABC-water systems. Therefore, the χ parameter at higher temperature decreases with rising temperature. It is noted that the χ parameter decreases as a function of $1/RT$ with increasing temperature when the interaction energies of polymer-polymer, polymer-solvent, and solvent-solvent do not depend on temperature. Only LCST type phase separation was observed for previously investigated AEC with higher DS, suggesting more significant increase of χ with dehydration around LCST. This prediction is of interest to explore new thermosensitive polymers with closed-loop phase diagram.

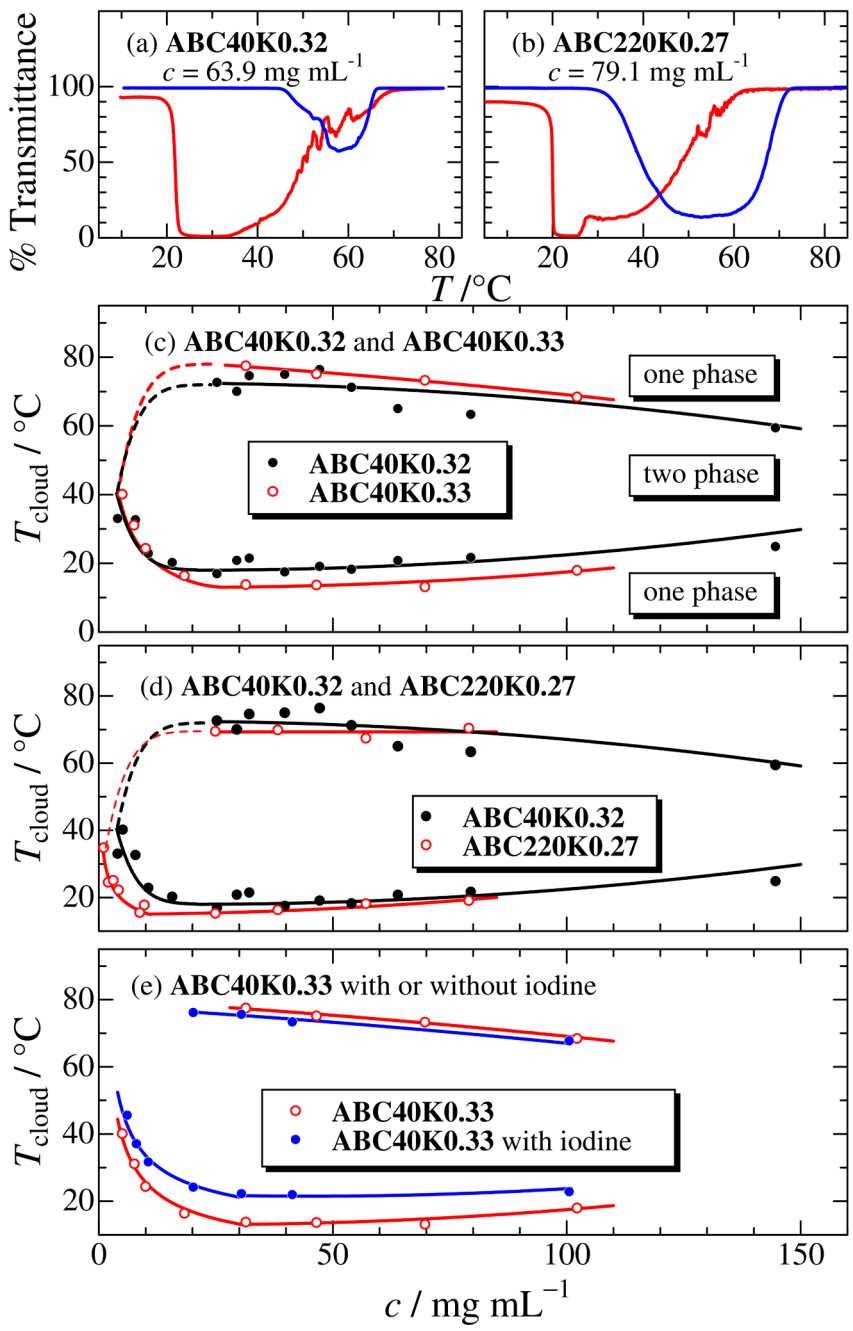

Fig. 3. (a) (b) Results from phase separation experiments. Temperature course of the optical transmittance at heating (red) and cooling (blue) processes. Both heating and cooling rate, 0.5 °C min^{-1}. (c) (d) Phase diagrams for the indicated ABC samples in water. Cloud point temperatures T_{cloud} are plotted against polymer mass concentration c. (e) Phase diagram for **ABC40K0.33** in water with or without iodine. Concentration of iodine is about 0.3 mM.

3.3. Inclusion complex formation behavior with iodine

As in the case of starch or amylose, we reported that AEC samples have inclusion complex formation ability with iodine. Fig. 4 shows the result for the iodine test; panel (a) indicates the wavelength λ_0 dependence of the molar absorption coefficient ε of iodine. All water-soluble ABC samples have significant absorption in the visible light wavelength range, indicating appreciable complex formation ability with iodine in water. It is noted that much smaller absorption of iodine was observed without ABC. As shown in panel (b), peak height decreases with increasing temperature and almost vanishes at 80 °C. This is most likely due to the dissociation of the ABC-iodine complexes with increasing temperature. Similar temperature variation is also known for the starch-iodine system. The peak wavelength $\lambda_{0,peak}$ is plotted against DS in Fig. 4(c). The $\lambda_{0,peak}$ values for the current ABC samples are well-fitted by the straight line for the previously investigated AEC samples. This indicates that the complex formation ability of AEC and ABC is quite similar. However, the DS range of thermo-responsive ABC is substantially lower than that of AEC. In other words, thermoresponsive ABC samples (DS ~ 0.3) exhibit a complex formation ability with iodine more similar to amylose than that of thermoresponsive AEC samples (DS ~ 1).

Complexation of ABC with small molecules may influence the phase separation behavior. Fig 3(e) compares the phase diagram of **ABC40K0.33** – water system with or without iodine. While the T_{cloud} values for the upper phase boundaries (UCST) are not affected by iodine, the T_{cloud} value for the lower phase boundary (LCST) with iodine is appreciably higher than that without iodine. This is consistent with that complex formation is only significant at low temperatures and the electrostatic repulsion of the negatively charged I_3^- or I_5^- ions confined in the helical structure of ABC gives better solubility in water than ABC without iodine. Similar behavior only for the LCST was also observed for AEC-iodine system

(Kimura et al., 2020) and the polymeric crown ethers – potassium ion systems (Huang et al., 2018).

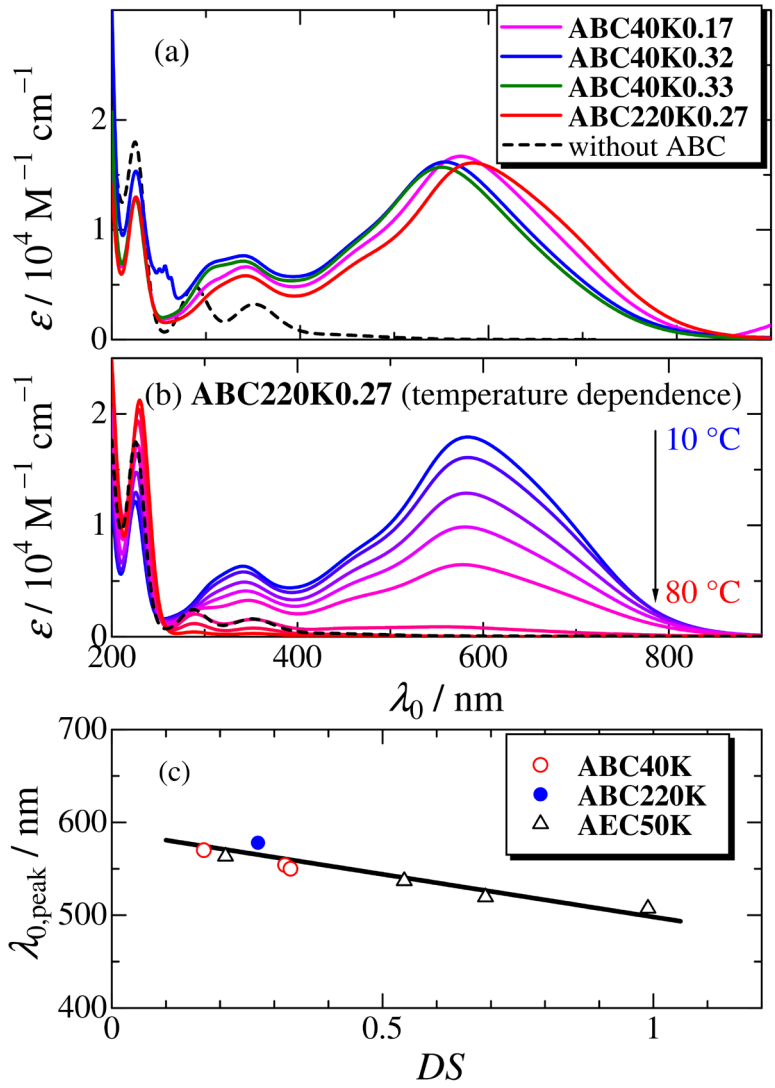

Fig. 4. (a) UV-Vis absorption spectra for the indicated ABC samples in water. c = 5 mg mL^{-1} at 20 °C. Iodine concentration, 0.3 mM. (b) UV-Vis absorption spectra for **ABC220K0.27** at different temperatures. Concentrations are the same as that in panel (a). (c) Degree of substitution DS dependences of the peak wavelength $\lambda_{0,peak}$ for the ABC samples at 20 °C along with those for previously investigated partially substituted amylose ethylcarbamates (AEC50K) samples at 25 °C (Kimura et al., 2020).

4. Conclusions

A dual-thermoresponsive polysaccharide derivative, specifically polysaccharide derivatives exhibiting both UCST and LCST type phase separation behavior in aqueous solution, has been successfully achieved with partially substituted amylose butylcarbamate (ABC). At least in the narrow sense, excluding sol-gel transitions, this is a novel finding for polysaccharide derivatives. The degree of substitution DS of the thermoresponsive ABC samples are about 0.3, which is about 1/3 – 1/4 times smaller than that of previously investigated amylose ethylcarbamate (AEC) exhibiting LCST type phase separation behavior. The LCST and UCST can be changed both by the chain length and DS between 13 – 17 °C and 70 – 77 °C, respectively. The closed-loop phase diagram was also confirmed by that an ABC solution with c = 3 mg mL^{-1} is stable even between UCST and LCST and the chain conformation is almost independent of the temperature. Appreciable inclusion complex formation behavior was observed for water-soluble ABC samples. The absorption wavelength is consistent with the previously investigated AEC sample with the same DS. Considering the low DS for the thermoresponsive ABC, it can be a better source for the thermoresponsive material compared to the other polysaccharide derivatives, many of which have DS values greater than unity. Another important finding is that the DS range to achieve dual thermoresponsive nature is quite narrow. This is because the change in interaction parameter with dehydration at LCST should not be significant to achieve UCST at higher temperatures. These findings lead us to expect that similar phase separation behavior is hidden in many polysaccharide derivatives.

Supporting Information

Additional figures for chemical reaction formula, ^{1}H-NMR, DLS, and SAXS data.

Acknowledgments

The authors are grateful to Dr. Noboru Ohta (SPring-8) for SAXS measurements. The synchrotron radiation experiments were performed at the BL40B2 in SPring-8 with the approval of the Japan Synchrotron Radiation Research Institute (JASRI) (proposal Nos. 2020A0529, 2021A1092, 2021B1138, 2021B1139, 2022A1083, 2022B1119, 2022B1120). This work was the result of using research equipment (NMR and ultimate analysis) shared in MEXT Project for promoting public utilization of advanced research infrastructure (Program for supporting construction of core facilities) Grant No. JPMXS0441200021 and JPMXS0441200022. This work was partly supported by JSPS KAKENHI grant Nos. JP20H02788 and JP23H02011.

References

Audureau, N., Coumes, F., Rieger, J., & Stoffelbach, F. (2022). Poly(N-cyanoethylacrylamide), a new thermoresponsive homopolymer presenting both LCST and UCST behavior in water. *Polymer Chemistry,* 13(8), 1075-1083.

Benoit, H., & Doty, P. (1953). Light Scattering from Non-Gaussian Chains. *The Journal of Physical Chemistry,* 57(9), 958-963.

Bizmark, N., Caggiano, N. J., Liu, J. X., Arnold, C. B., Prud'homme, R. K., Datta, S. S., & Priestley, R. D. (2022). Hysteresis in the thermally induced phase transition of cellulose ethers. *Soft Matter,* 18(33), 6254-6263.

Burchard, W., & Kajiwara, K. (1970). The statistics of stiff chain molecules I. The particle scattering factor. *Proceedings of the Royal Society of London. A. Mathematical and Physical Sciences,* 316(1525), 185-199.

Cai, X., Zhong, L., Su, Y., Lin, S. L., & He, X. H. (2015). Novel pH-tunable thermoresponsive polymers displaying lower and upper critical solution temperatures. *Polymer Chemistry,* 6(20), 3875-3884.

Cardoso, M. B., Putaux, J. L., Nishiyama, Y., Helbert, W., Hytch, M., Silveira, N. P., & Chanzy, H. (2007). Single crystals of V-amylose complexed with alpha-naphthol. *Biomacromolecules,* 8(4), 1319-1326.

Chen, C., Zhang, W., Zhang, Y., Wang, P., & Ren, F. (2022). Tunable Thermo-Responsive Properties of Hydroxybutyl Chitosan Oligosaccharide. *Front Chem,* 10, 830516.

Chevillard, C., & Axelos, M. A. V. (1997). Phase separation of aqueous solution of methylcellulose. *Colloid and Polymer Science,* 275(6), 537-545.

Glatter, O., & Kratky, O. (1982). *Small Angle X-ray Scattering*. London: Academic Press.

Han, J., Takahashi, R., Kuang, C., & Sato, T. (2022). Phase Separation Behavior of Aqueous Poly(N-isopropylacrylamide) Solutions Studied by Scattering Experiments. *Langmuir,* 38(17), 5089-5097.

Heymann, E. (1935). Studies on sol-gel transformations. I. The inverse sol-gel transformation of methylcellulose in water. *Transactions of the Faraday Society,* 31(1), 0846-0863.

Huang, D. C., Zhang, Q., Deng, Y., Luo, Z., Li, B., Shen, X., . . . Chen, W. (2018). Polymeric crown ethers: LCST behavior in water and stimuli-responsiveness. *Polymer Chemistry,* 9(19), 2574-2579.

Jiang, X. Y., Kitamura, S., Sato, T., & Terao, K. (2017). Chain Dimensions and Stiffness of Cellulosic and Amylosic Chains in an Ionic Liquid: Cellulose, Amylose, and an Amylose Carbamate in BmimCl. *Macromolecules,* 50(10), 3979-3985.

Ju, B., Cao, S., & Zhang, S. (2013). Effect of additives on the cloud point temperature of 2-hydroxy-3-isopropoxypropyl starch solutions. *Journal of Physical Chemistry B,* 117(39), 11830-11835.

Ju, B. Z., Yan, D. M., & Zhang, S. F. (2012). Micelles self-assembled from thermoresponsive 2-hydroxy-3-butoxypropyl starches for drug delivery. *Carbohydrate Polymers,* 87(2), 1404-1409.

Kabata, D., Ryoki, A., Kitamura, S., & Terao, K. (2021). Chain Alignment of a Rigid Ring Polymer in the Lyotropic Liquid Crystal Phase: Cyclic Amylose Tris(n-butylcarbamate) in Tetrahydrofuran and Ethyl Lactate. *Macromolecules,* 54(23), 10723-10729.

Kimura, S., Kochi, R., Kitamura, S., & Terao, K. (2020). A Temperature Responsive Polysaccharide Derivative in Aqueous Solution: Amylose Ethyl Carbamates. *Acs Applied Polymer Materials,* 2(6), 2426-2433.

Kitamura, S., Yunokawa, H., Mitsuie, S., & Kuge, T. (1982). Study on Polysaccharide by the Fluorescence Method .2. Micro-Brownian Motion and Conformational Change of Amylose in Aqueous-Solution. *Polymer Journal,* 14(2), 93-99.

Le, C. A. K., Ogawa, Y., Grimaud, F., Nishiyama, Y., Morfin, I., Potocki-Veronese, G., . . . Putaux, J. L. (2022). Helical Inclusion Complexes of Amylose with Aromatic Compounds: Crystallographic Evidence for New V-Type Allomorphs. *Crystal Growth & Design,* 22(12), 7079-7089.

Li, M. J., He, X. L., Ling, Y., & Tang, H. Y. (2017). Dual thermoresponsive homopolypeptide with LCST-type linkages and UCST-type pendants: Synthesis, characterization, and thermoresponsive properties. *Polymer,* 132, 264-272.

Liu, R. X., Fraylich, M., & Saunders, B. R. (2009). Thermoresponsive copolymers: from fundamental studies to applications. *Colloid and Polymer Science,* 287(6), 627-643.

Longenecker, R., Mu, T. T., Hanna, M., Burke, N. A. D., & Stover, H. D. H. (2011). Thermally Responsive 2-Hydroxyethyl Methacrylate Polymers: Soluble-Insoluble and Soluble-Insoluble-Soluble Transitions. *Macromolecules,* 44(22), 8962-8971.

McAllister, J. W., Schmidt, P. W., Dorfman, K. D., Lodge, T. P., & Bates, F. S. (2015). Thermodynamics of Aqueous Methylcellulose Solutions. *Macromolecules,* 48(19), 7205-7215.

Nakamura, Y., & Norisuye, T. (2004). Scattering function for wormlike chains with finite thickness. *Journal of Polymer Science Part B-Polymer Physics,* 42(8), 1398-1407.

Nakamura, Y., & Norisuye, T. (2008). *Brush-like polymers*. In R. Borsali & R. Pecora (Eds.), *Soft Matter Characterization* (pp. 235-286): Springer Netherlands

Nishida, K., Morita, H., Katayama, Y., Inoue, R., Kanaya, T., Sadakane, K., & Seto, H. (2017). Salting-out and salting-in effects of amphiphilic salt on cloud point of aqueous methylcellulose. *Process Biochemistry,* 59, 52-57.

Nishiyama, Y., Mazeau, K., Morin, M., Cardoso, M. B., Chanzy, H., & Putaux, J. L. (2010). Molecular and Crystal Structure of 7-Fold V-Amylose Complexed with 2-Propanol. *Macromolecules,* 43(20), 8628-8636.

Norisuye, T., & Fujita, H. (1982). Excluded-Volume Effects in Dilute Polymer Solutions. XIII. Effects of Chain Stiffness. *Polymer Journal,* 14(2), 143-147.

Norisuye, T., Tsuboi, A., & Teramoto, A. (1996). Remarks on Excluded-Volume Effects in Semiflexible Polymer Solutions. *Polymer Journal,* 28(4), 357-361.

Okamura, H., Maruyama, T., Masuda, S., Minagawa, K., Mori, T., & Tanaka, M. (2002). *Journal of Polymer Research,* 9(1), 17-21.

Otto, S., Marina, P. F., Zhou, F., & Blencowe, A. (2021). Thermoresponsive polysaccharides with tunable thermoresponsive properties via functionalisation with alkylamide groups. *Carbohydrate Polymers,* 254, 117280.

Phunpee, S., Ruktanonchai, U. R., & Chirachanchai, S. (2022). Tailoring a UCST-LCST-pH Multiresponsive Window through a Single Polymer Complex of Chitosan-Hyaluronic Acid. *Biomacromolecules,* 23(12), 5361-5372.

Roy, D., Brooks, W. L., & Sumerlin, B. S. (2013). New directions in thermoresponsive polymers. *Chemical Society Reviews,* 42(17), 7214-7243.

Saeki, S., Kuwahara, N., Nakata, M., & Kaneko, M. (1976). Upper and lower critical solution temperatures in poly (ethylene glycol) solutions. *Polymer,* 17(8), 685-689.

Sarkar, N. (1979). Thermal Gelation Properties of Methyl and Hydroxypropyl Methylcellulose. *Journal of Applied Polymer Science,* 24(4), 1073-1087.

Shimizu, N., Yatabe, K., Nagatani, Y., Saijyo, S., Kosuge, T., & Igarashi, N. (2016). Software Development for Analysis of Small-angle X-ray Scattering Data. *AIP Conference Proceedings,* 1741(1), 050017.

Shiomi, T., Imai, K., Watanabe, C., & Miya, M. (1984). Thermodynamic and conformational properties of partially butyralized poly(vinyl alcohol) in aqueous solution. *Journal of Polymer Science: Polymer Physics Edition,* 22(7), 1305-1312.

Shirakawa, M., Yamatoya, K., & Nishinari, K. (1998). Tailoring of xyloglucan properties using an enzyme. *Food Hydrocolloids,* 12(1), 25-28.

Terao, K., Maeda, F., Oyamada, K., Ochiai, T., Kitamura, S., & Sato, T. (2012). Side-chain-dependent helical conformation of amylose alkylcarbamates: amylose tris(ethylcarbamate) and amylose tris(n-hexylcarbamate). *Journal of Physical Chemistry B,* 116(42), 12714-12720.

Terao, K., Murashima, M., Sano, Y., Arakawa, S., Kitamura, S., & Norisuye, T. (2010). Conformational, Dimensional, and Hydrodynamic Properties of Amylose Tris(*n*-butylcarbamate) in Tetrahydrofuran, Methanol, and Their Mixtures. *Macromolecules,* 43(2), 1061-1068.

Terao, K., & Sato, T. (2018). *Conformational Properties of Polysaccharide Derivatives*. In G. Yang & L. Lamboni (Eds.), *Bioinspired Materials Science and Engineering* (pp. 167-183)

Tomofuji, Y., Yoshiba, K., Christensen, B. E., & Terao, K. (2019). Single-chain conformation of carboxylated schizophyllan, a triple helical polysaccharide, in dilute alkaline aqueous solution. *Polymer,* 185, 121944.

Wang, X. H., Qiu, X. P., & Wu, C. (1998). Comparison of the coil-to-globule and the globule-to-coil transitions of a single poly(N-isopropylacrylamide) homopolymer chain in water. *Macromolecules,* 31(9), 2972-2976.

Wu, C., & Wang, X. H. (1998). Globule-to-coil transition of a single homopolymer chain in solution. *Physical Review Letters,* 80(18), 4092-4094.

Yamakawa, H., & Yoshizaki, T. (2016). *Helical Wormlike Chains in Polymer Solutions, 2nd ed.* Berlin, Germany: Springer.

Zhu, Y. C., Batchelor, R., Lowe, A. B., & Roth, P. J. (2016). Design of Thermoresponsive Polymers with Aqueous LCST, UCST, or Both: Modification of a Reactive Poly(2-vinyl-4,4-dimethylazIactone) Scaffold. *Macromolecules,* 49(2), 672-680.

Supporting Information for

Dual thermoresponsive polysaccharide derivative – water system. Partly substituted amylose *n*-butylcarbamate in water

Yuma Nakata,[a] Shinichi Kitamura,[b] and Ken Terao*,[a]

[a]Department of Macromolecular Science, Graduate School of Science, Osaka University, 1-1 Machikaneyama-cho, Toyonaka, Osaka 560-0043, Japan

[b]Center for Research and Development of Bioresources, Organization for Research Promotion, Osaka Prefecture University1-2, Gakuen-cho, Naka-ku, Sakai 599-8570, Japan

* Corresponding author. E-mail address: terao.ken.sci@osaka-u.ac.jp

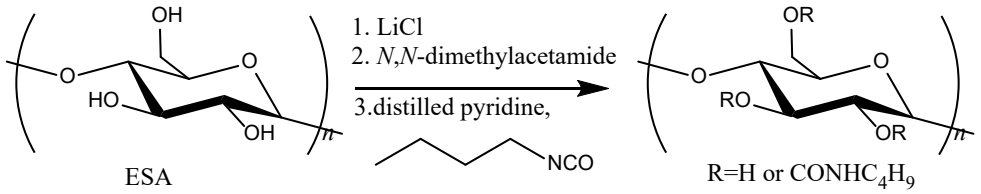

Fig. S1. Synthesis of partly substituted amylose butylcarbamate (ABC) from enzymatically synthesized amylose ESA.

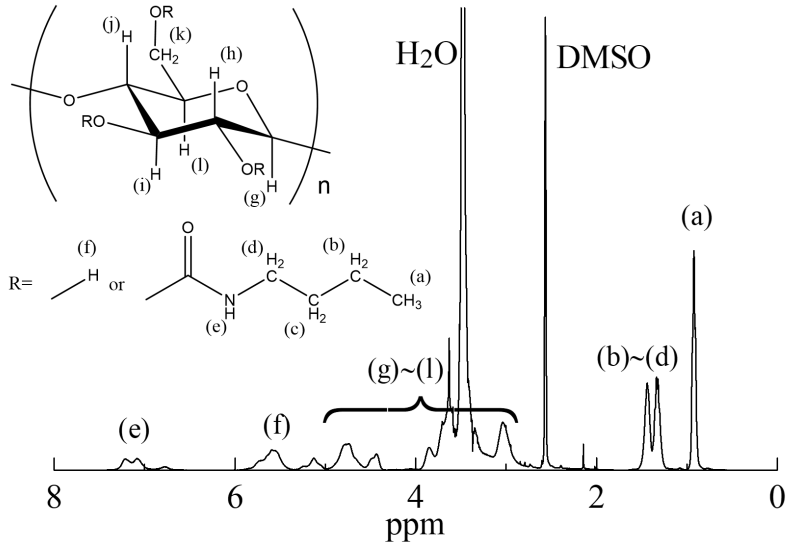

Fig. S2. A ^{1}H NMR-spectrum of **ABC40K0.83** in DMSO-d6 25 °C.

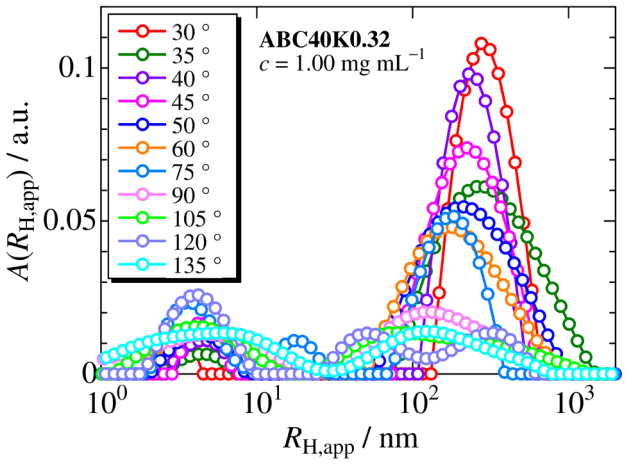

Fig. S3. Example of DLS results for a **ABC40K0.32** solution (c = 1.00 mg mL^{-1}) in water at 10 °C detected at the indicated scattering angles.

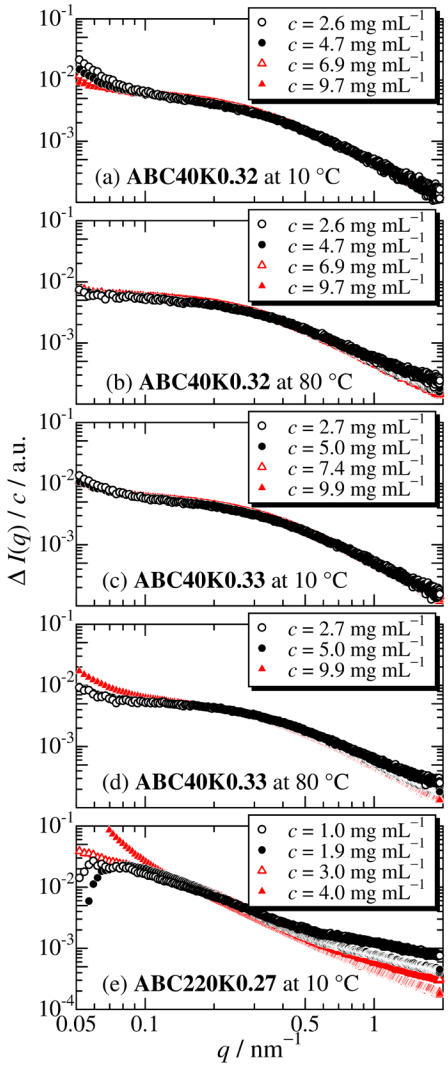

Fig. S4. SAXS raw data for ABC samples in water. Double logarithmic plots of the excess scattering intensity $\Delta I(q)$ divided by the polymer mass concentration c vs the magnitude q of the scattering vector.